

# Journal of Materials Chemistry A

Accepted Manuscript



This is an *Accepted Manuscript*, which has been through the Royal Society of Chemistry peer review process and has been accepted for publication.

*Accepted Manuscripts* are published online shortly after acceptance, before technical editing, formatting and proof reading. Using this free service, authors can make their results available to the community, in citable form, before we publish the edited article. We will replace this *Accepted Manuscript* with the edited and formatted *Advance Article* as soon as it is available.

You can find more information about *Accepted Manuscripts* in the [Information for Authors](#).

Please note that technical editing may introduce minor changes to the text and/or graphics, which may alter content. The journal's standard [Terms & Conditions](#) and the [Ethical guidelines](#) still apply. In no event shall the Royal Society of Chemistry be held responsible for any errors or omissions in this *Accepted Manuscript* or any consequences arising from the use of any information it contains.



Journal Name

ARTICLE

## Dual Catalytic Behaviors of a Soluble Ferrocene as Electrocatalyst and Electrochemistry for Na-air Battery

Wen-Wen Yin<sup>ab</sup>, Ji-Li Yue<sup>a</sup>, Ming-Hui Cao<sup>a</sup>, Wen Liu<sup>a</sup>, Jing-Jing Ding<sup>a</sup>, Fei Ding<sup>b</sup>, Lin Sang<sup>b</sup>, Zheng-Wen Fu<sup>a</sup>

Received 00th January 20xx,  
Accepted 00th January 20xx

DOI: 10.1039/x0xx00000x

www.rsc.org/

Metal-air batteries are important power sources for electronics and vehicles because of their remarkable high theoretical energy density and low cost. In this work, we firstly investigate the electrochemical properties of sodium air batteries (SABs) with the addition of ferrocene in the electrolyte. Combined charge-discharge measurements with Field-emission transmission electron microscopy images of the discharged air cathodes, our results have demonstrated that two different pathways with ferrocene as electrocatalyst and electrochemistry during the charge process might be governed by the morphological feature of the electrode caused by the deposition of Na<sub>2</sub>O<sub>2</sub> in SABs. The SAB with ferrocene as catalyst exhibits a highly cycling performance of up to 230 cycles with a high capacity of 1000 mAh g<sup>-1</sup>.

### Introduction

The high price more than \$500 kWh<sup>-1</sup> of battery packs for electric cars is the main obstacle for their mass uses. There is an urgent need to develop clean and cheap energy sources for electric vehicles. Rechargeable SABs have the merits of being environment friendly and low cost close to \$100 kWh<sup>-1</sup>; they are deemed the better chance of meeting the economics needed to compete with conventional cars.<sup>1</sup> However, there was not concerned work about the sodium air batteries until 2011. After the feasibility of running a liquid SAB at above 100 °C was introduced by Peled *et al.*,<sup>2</sup> our group reported the rechargeable SABs working at room temperature for the first time.<sup>3</sup> Over the past few years, the major objectives of researchers in this field were identifying new catalyst materials and improving their performance for the future development of SABs. In 2013, we found that Graphene nanosheets (GNSs) employed as air electrodes, the SABs can achieve high discharge capacity of 8268 mAh g<sup>-1</sup> at the current density of 200 mA g<sup>-1</sup>, which is superior to that of the carbon electrode. However, the insoluble discharge products accumulated onto the porous network of the GNS cathodes after the 10 cycles, leading to the increasing discharge and charge polarizations.<sup>4</sup> Li *et al.* demonstrated that nitrogen-doped graphene nanosheets (N-GNSs) served as cathode materials delivered a discharge capacity two times greater than that for GNSs.<sup>5</sup> Although the defective sites generated after doping nitrogen into GNSs are conducive to the formation of discharge products, the

cyclic performance is still unsatisfactory. Jian *et al.* directly used a 3D interpenetrating CNT paper as a binder-free cathode in the SABs, the overpotential gap is as small as 200 mV with the Na<sub>2</sub>O<sub>2</sub>·2H<sub>2</sub>O identified as the main discharge product.<sup>6</sup> By employing NiCo<sub>2</sub>O<sub>4</sub> nanosheets supported on Ni foam as air catalysts, the battery exhibited 10 cycles at a constant current density of 50 mA g<sup>-1</sup> between 1.8 and 4.0 V.<sup>7</sup> Rosenberg *et al.* prepared α-MnO<sub>2</sub> nanowires as catalyst materials in the SABs. In their work, the batteries remained approximately 85% of the initial specific charge after 55 cycles.<sup>8</sup> Hartmann *et al.* reported on a Na-O<sub>2</sub> cell reversibly discharging/charging at very low overpotentials (<200mV) with crystalline sodium superoxide (NaO<sub>2</sub>) formed as a solid discharge product for the first time under flushed with oxygen for 10s at 10<sup>5</sup> Pa.<sup>9-11</sup> Their breakthrough results have shown that the shallow overpotential can improve the cycle life of the batteries with stable capacity values of 64 mAh g<sup>-1</sup> for at least 80 cycles using a carbon-fibre gas diffusion layer and 1666 mAh g<sup>-1</sup> for at least 60 cycles using Ketjenblack as air cathodes.<sup>12</sup> By manipulating the nucleation and growth of nano-sized NaO<sub>2</sub> particles in a VACNT network with a large surface area, the electrical energy efficiency of Na-O<sub>2</sub> cells as high as 90% for up to 100 cycles is achieved by Zhao *et al.*<sup>13</sup> Nevertheless, the fading becomes more and more prevalent as the number of cycles increases. In the above reports, since the decomposition of discharge products was electrochemically driven by carbon or other solid catalysts, which cannot sufficiently facilitate the decomposition of nonconductive discharge products, thus induce the degradation of the cells and the best cyclic performance of the SABs is just 100 cycles.

While, soluble catalysts homogeneous dissolving in the electrolytes can provide oxidative attack at the much larger and dynamic interphase between discharge products and the liquid electrolyte, then improving the cyclic performance of the SABs. Recently, we have introduced NaI, a new soluble catalyst, for the SABs, the cyclic performance of which can achieve 150 cycles. Our work demonstrates that the soluble catalyst can effectively enhance

<sup>a</sup>Shanghai Key Laboratory of Molecular Catalysts and Innovative Materials, Department of Chemistry & Laser Chemistry Institute, Fudan University, Shanghai 200433, P.R. China. E-mail address: zwfu@fudan.edu.cn

<sup>b</sup>National Key Laboratory of Science and Technology on Power Sources, Tianjin Institute of Power Sources, Tianjin 300384, P. R. China

† Electronic Supplementary Information (ESI) available: [Discharge & charge profiles of the cell in Fe(C<sub>5</sub>H<sub>5</sub>)<sub>2</sub>-containing electrolyte and UV absorption spectra]. See DOI: 10.1039/x0xx00000x

the cyclability of the SABs. However, the volatilization of iodine in the two-electrode cell during the cycling process ultimately resulted in the deterioration of the electrochemical performance.<sup>14</sup> Herein, a new nonvolatile and soluble catalyst of ferrocene is utilized in the SABs. The electrochemical performance of SABs with the ferrocene as the soluble catalyst will be examined and its catalytic mechanism will be investigated.

## Results and discussion

The discharge and charge curves of SABs by using liquid electrolytes without and with ferrocene ( $\text{Fe}(\text{C}_5\text{H}_5)_2$ ) were measured at room temperature and illustrated in Fig.1a. The specific capacity of the battery with a CNT@Ni cathode is based on the mass of CNT. The battery using the electrolyte without the addition of  $\text{Fe}(\text{C}_5\text{H}_5)_2$  is charged at a fixed voltage of 3.8 V, while, the battery using the liquid electrolyte with the addition of  $\text{Fe}(\text{C}_5\text{H}_5)_2$  is charged at the depth of discharge (DOD) with a capacity cut-off. It can be seen that the addition of ferrocene has little effect on the discharge curves. The discharge plateaus of CNT@Ni air electrode in the electrolyte without and with the addition of  $\text{Fe}(\text{C}_5\text{H}_5)_2$  are both at about 2.1 V. It seems that the ferrocene is irrelevant to the ORR (oxygen reduction reaction), which still needs further study. Interestingly, a reduction of charging potential is found in the  $\text{Fe}(\text{C}_5\text{H}_5)_2$ -containing electrolyte. The first charge curve is characterized by a sloping voltage plateau from 2.2 to 2.8 V and a flat voltage plateau at 3.1 V, implying two different pathways in the charge process. The significantly reduced charging voltage in the presence of  $\text{Fe}(\text{C}_5\text{H}_5)_2$  leads to a distinct improvement in the cyclic performance of the cells, as shown in Fig.1b-d and S1 with various concentrations of  $\text{Fe}(\text{C}_5\text{H}_5)_2$ -containing electrolytes. Their cyclability is strongly dependent on the concentration of  $\text{Fe}(\text{C}_5\text{H}_5)_2$  in the electrolyte. It should be noted that the feature of charge curves varies with the cycles (Fig.1b-d and S1). The charge curves of the cell with different concentration of ferrocene dissolving in the electrolyte consist of a sloping voltage plateau from 2.2 to 2.8 V and a flat voltage plateau at 3.1 V. While, the contribution of two

of the CNT@Ni electrode using (b) 0.01M (c) 0.05M (d) 0.10 M  $\text{Fe}(\text{C}_5\text{H}_5)_2$ -containing electrolyte (the capacity was limited to 1000  $\text{mA g}^{-1}$ ) at the current density of 500  $\text{mA g}^{-1}$ .

plateaus varies with the concentration of ferrocene, which still needs further investigation. Obviously, their cyclability is strongly dependent on the concentration of  $\text{Fe}(\text{C}_5\text{H}_5)_2$  in the electrolyte. The reversible and stable cycling of the cells, with 0.05M  $\text{Fe}(\text{C}_5\text{H}_5)_2$  in the electrolyte, up to 230 cycles is observed, which is the best in the cycle performance of SABs reported previously. In the charge process, the capacity of a slope from 2.0 V to 2.8 V gradually increases with cycles, while that of the flat voltage plateau at 3.1 V becomes shorter and ultimately disappears after the 200<sup>th</sup> cycle (Fig.1c). Although the cell using the  $\text{Fe}(\text{C}_5\text{H}_5)_2$ -containing electrolyte shows similar discharge voltage profiles, the voltage polarization during the discharge process increases with cycle numbers. It can be clearly seen that the initial discharge and charge profiles are utterly different from those of 200<sup>th</sup>-230<sup>th</sup> cycles. Both the terminal voltage of the discharge process and the voltage gap at 500  $\text{mA h g}^{-1}$  decrease with the increasing cycle, as indicated in Fig.2a. The voltage gap at 500  $\text{mA h g}^{-1}$  between galvanostatic discharge and charge during 1<sup>st</sup> cycle is 780 mV, while, it is just 350 mV in the 230<sup>th</sup> cycle (S2). Both the voltage gap of 350 mV and the charging potential (Tab.S1) are lower than that in previous reports applying N-GNS or other air electrode catalysts in SABs with  $\text{Na}_2\text{O}_2$ <sup>5,6,13</sup> as the discharge product, but higher than that with the  $\text{NaO}_2$ <sup>7-11</sup> as the discharge product. These results indicate that the air electrode based a soluble ferrocene displays an exceedingly high electrocatalytic activity for OER (oxygen evolution reaction).

To gain an insight into the mechanism of the discharge and charge processes, galvanostatic intermittent titration technique (GITT) was tested at a current density of 500  $\text{mA g}^{-1}$  for 1h followed by a relaxation time 10 h. As shown in Fig.2b, the equilibrium voltages ( $U_{\text{eq}}$ ) of discharge and charge processes can nearly reach the same  $U_{\text{eq}}$  of 2.27 V, which coincides with the  $U_{\text{eq}}$  for the formation of  $\text{Na}_2\text{O}_2$ .<sup>15</sup> Undoubtedly, the discharge process in the  $\text{Fe}(\text{C}_5\text{H}_5)_2$ -containing electrolyte accords with the feature of SABs. While, the flat voltage plateau (3.1V) is close to the theoretical oxidation potential of  $\text{Fe}(\text{C}_5\text{H}_5)_2^+ / \text{Fe}(\text{C}_5\text{H}_5)_2$  (3.4V). It should be reasonably assumed that the high charge voltage plateau of 3.1 V can mainly be attributed to the electrochemical oxidation of  $\text{Fe}(\text{C}_5\text{H}_5)_2$ .

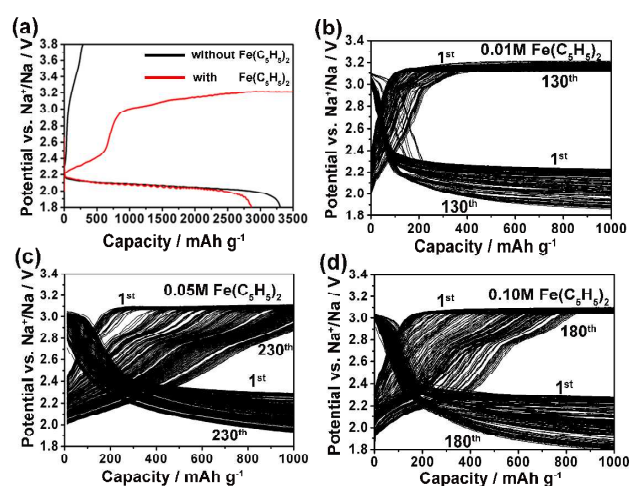


**Fig. 1** (a) Initial discharge-charge profiles of CNT@Ni cathodes obtained by using liquid electrolytes without and with  $\text{Fe}(\text{C}_5\text{H}_5)_2$ , at the current density of 500  $\text{mA g}^{-1}$ , respectively. Cyclic performance

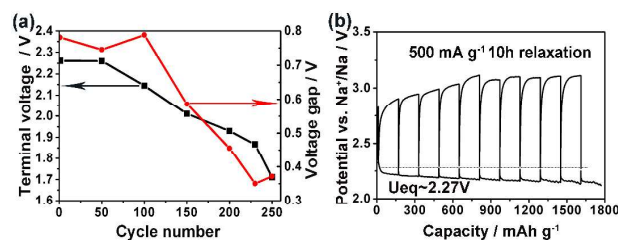


**Fig. 2** (a) Terminal discharge voltage (the black line) and voltage gap (the red line) during galvanostatic discharge and charge at 500  $\text{mA h g}^{-1}$  as a function of cycle numbers. (b) GITT curves plotted with the voltage as a function of specific capacity.

In order to further clarify the discharge-charge process in the

SABs, the air electrodes in the 0.05M  $\text{Fe}(\text{C}_5\text{H}_5)_2$ -containing electrolyte before and after the initial discharge and charge processes were characterized and compared by using *ex situ* TEM and SAED techniques. The SAB was first discharged to 1.8 V and then charged to 3.3 V at a constant current of 100 mA  $\text{g}^{-1}$ . The typical TEM images of the air electrodes are shown in Fig. 3a-b. It can be seen that the diameter of the CNT is about 30 nm in Fig.3b. The SAED pattern of the pristine electrode material shown in Fig. 3c consists of one brighter and one dark rings, both of which could be indexed to the CNT. After the cell was discharged to 1.8 V, the HRTEM image shows that an ultra-thin film of the product is attached on the CNT (labeled by the white arrow shown in Fig.3d), and the crystallites with clear and coherent stripes are observed in enlarged HRTEM images as shown in Fig.3e. The corresponding SAED pattern exhibits clear concentric rings, indicating the nanosized polycrystalline nature of the discharge product (Fig.3f). All diffraction d-spacings in the SAED pattern can be well indexed to hexagonal  $\text{Na}_2\text{O}_2$  (JCPDS CardNo.74-895). These results indicate that nanocrystalline  $\text{Na}_2\text{O}_2$  is formed when the cell is discharged to 1.8 V. Upon charging,  $\text{Na}_2\text{O}_2$  is completely removed from the CNT electrode as shown in Fig.3e, indicating a high reversibility of the air electrode. The diffraction patterns in Fig.3f also confirm the absence of  $\text{Na}_2\text{O}_2$  after charging.

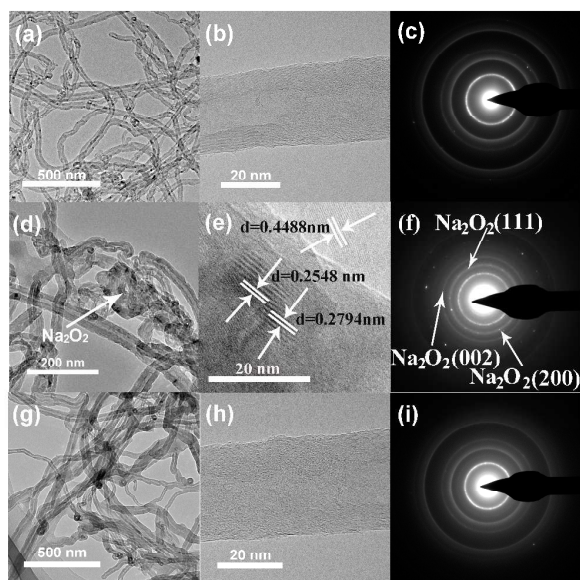


**Fig. 3** High resolution TEM images of the air electrodes: (a) (b) before and (d) (e) after initially discharging the battery to 1.8 V; (g) and (h) after initially charging the battery to 3.3 V at a constant current of 100 mA  $\text{g}^{-1}$ ; and (c) (f) and (i) their corresponding SAED patterns, respectively.

The FESEM images of the pristine air cathode (Fig.4a), the discharged air cathodes after 1<sup>st</sup> (Fig.4b), 200<sup>th</sup> (Fig.4c), 230<sup>th</sup> (Fig.4d) cycles were measured to further clarify the origin of the difference in the charge processes. As shown in Fig.4a, the pristine cathode consists of uniform carbon nanotubes. However, after 1<sup>st</sup> cycle, the porous layers products ( $\text{Na}_2\text{O}_2$ ) are formed and not fully cover onto

the discharged air cathode (Fig.4b). Compared with the image of the air cathode after the initial cycle, these of the air cathodes after the 200<sup>th</sup> cycles take on completely different appearances, the discharge product on the surface of air electrode becomes so dense that the air cathode is completely covered. In other words, the morphologies of  $\text{Na}_2\text{O}_2$  depend on the cycle numbers. The morphological evolution of  $\text{Na}_2\text{O}_2$  should be related to the different charge curves during the cycles.

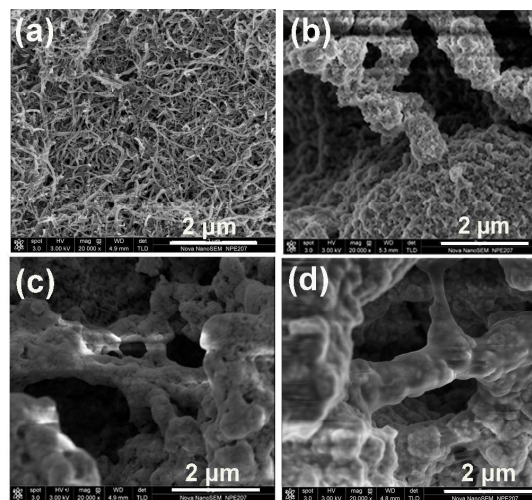


**Fig. 4** The SEM images of (a) the pristine air cathode, the discharged air cathodes after (b) 1<sup>st</sup> (c) 200<sup>th</sup> (d) 230<sup>th</sup> cycles.

To reveal the nature of  $\text{Fe}(\text{C}_5\text{H}_5)_2$  as a catalyst in the SABs, the composition of electrolytes containing 0.05M  $\text{Fe}(\text{C}_5\text{H}_5)_2$  in the SABs were examined by using UV spectroscopy when the battery was directly charged to 3.5 V, and the battery was discharged to 1.8 V and subsequently re-charged to 3.5 V, respectively, as shown in Fig.5a. The datum of solution containing  $\text{Fe}(\text{C}_5\text{H}_5)_2^+$  obtained by the reaction between  $\text{FeCl}_3$  and  $\text{Fe}(\text{C}_5\text{H}_5)_2$  in a faintly acid environment was also included for comparison. It can be seen that the  $\text{Fe}(\text{C}_5\text{H}_5)_2^+$  has a strong absorption at 619 nm, which is in accordance with the previous report.<sup>16</sup> An obvious absorption peak at 619 nm in the electrolyte containing  $\text{Fe}(\text{C}_5\text{H}_5)_2$  appears after the battery is directly charged to 3.5 V. These results indicate the formation of  $\text{Fe}(\text{C}_5\text{H}_5)_2^+$  during the charging process, which should correspond to the oxidation of  $\text{Fe}(\text{C}_5\text{H}_5)_2$  to  $\text{Fe}(\text{C}_5\text{H}_5)_2^+$ . Nevertheless, no absorption peak at 619 nm is observed in the electrolytes containing  $\text{Fe}(\text{C}_5\text{H}_5)_2$  after the battery is discharged to 1.8 V and subsequently re-charged to 3.5 V, indicating that no trace of  $\text{Fe}(\text{C}_5\text{H}_5)_2^+$  is detected during the cycles. Apparently, the UV spectrum of the electrolytes containing  $\text{Fe}(\text{C}_5\text{H}_5)_2$  after the battery directly charged to 3.5 V is utterly different from that after the battery discharged to 1.8 V and subsequent re-charged to 3.5 V. It implies that  $\text{Fe}(\text{C}_5\text{H}_5)_2^+$  formed during the charging process may react with the discharged product of  $\text{Na}_2\text{O}_2$ . In order to confirm the reaction process, the battery is set to directly charge to 2.0 mAh and then UV absorption spectra of the electrolyte at the various discharged states were examined and illustrated in Fig.5b. It can be seen that the absorbance of  $\text{Fe}(\text{C}_5\text{H}_5)_2^+$  at 619 nm decreases gradually and finally disappears when the

battery is discharged to 2.0 mAh. This phenomenon is similar to that the absorbance of  $\text{Fe}(\text{C}_5\text{H}_5)_2^+$  at 619 nm decreases with the incremental amount of  $\text{Na}_2\text{O}_2$  into the electrolytes containing  $\text{Fe}(\text{C}_5\text{H}_5)_2^+$  (S3), indicating the chemical reaction between the redox mediator of  $\text{Fe}(\text{C}_5\text{H}_5)_2^+$  and  $\text{Na}_2\text{O}_2$ . Thus, the chemical reaction of  $\text{Na}_2\text{O}_2$  formed during the discharge process with  $\text{Fe}(\text{C}_5\text{H}_5)_2^+$  results in the decreasing absorbance of  $\text{Fe}(\text{C}_5\text{H}_5)_2^+$  at 619 nm.

The discharge curves exhibit the feature of the SABs with the discharge plateau at 2.1 V. The formation of  $\text{Na}_2\text{O}_2$  during the discharge process could be supported by the GITT data, HRTEM and SAED data. In air batteries, the air cathode is one of the factors that determines the performance of cells. It is mostly agreed that the surface area and volume of mesopores are the parameters that affect the discharge capacity.<sup>17-20</sup> The CNTs adhere to the Ni foam has greatly improved the electrical conductivity of the all CNT air electrode. Besides, the unfilled pores between the skeletons of the Ni foam guarantee that  $\text{O}_2$  could diffuse into the CNTs at various depths, thus facilitating ORR and discharge product deposition. While, the CNT/Ni air electrodes are not effective for the OER, the ferrocene can act as electrocatalyst and electrochemistry during the

charge process. The charge process consists of two pathways, which corresponds to a sloping voltage plateau from 2.0 to 2.8 V (Pathway I) and a flat voltage plateau at 3.1 V (Pathway II). The former should involve the decomposition process of  $\text{Na}_2\text{O}_2$  driven under the electrocatalytic effect of ferrocene (**electrocatalysis**), during which the ferrocene exhibits the superior OER electrocatalytic activity. The ferrocene loaded on the air electrode as an efficient catalyst like other materials<sup>4,5,8,21</sup> could reduce the overpotential of the charging processes (Tab.S1). The latter involves the electrochemical oxidation of  $\text{Fe}(\text{C}_5\text{H}_5)_2$  into  $\text{Fe}(\text{C}_5\text{H}_5)_2^+$  (**electrochemistry**), according to UV absorption spectra of the electrolytes containing  $\text{Fe}(\text{C}_5\text{H}_5)_2$  after the battery directly charged to 3.5 V, then the oxidized product ( $\text{Fe}(\text{C}_5\text{H}_5)_2^+$ ) will spontaneously react with  $\text{Na}_2\text{O}_2$  formed in the discharge process to re-produce  $\text{Fe}(\text{C}_5\text{H}_5)_2$  and release  $\text{O}_2$  at the air electrode side. As previously reported for air batteries in pure oxygen environment, the catalyst exhibits either the electrocatalytic properties<sup>7,22,23</sup> or electrochemistry<sup>14</sup>. While, the liquid redox catalyst of  $\text{Fe}(\text{C}_5\text{H}_5)_2$ , homogeneous dissolving in the electrolyte, possesses the feature of dual catalytic behaviors as electrocatalyst and electrochemistry. In addition, the lower charge potential at about 3.1-3.2 V can avoid the decomposition of electrolyte and thus prolong cycle life of SABs.

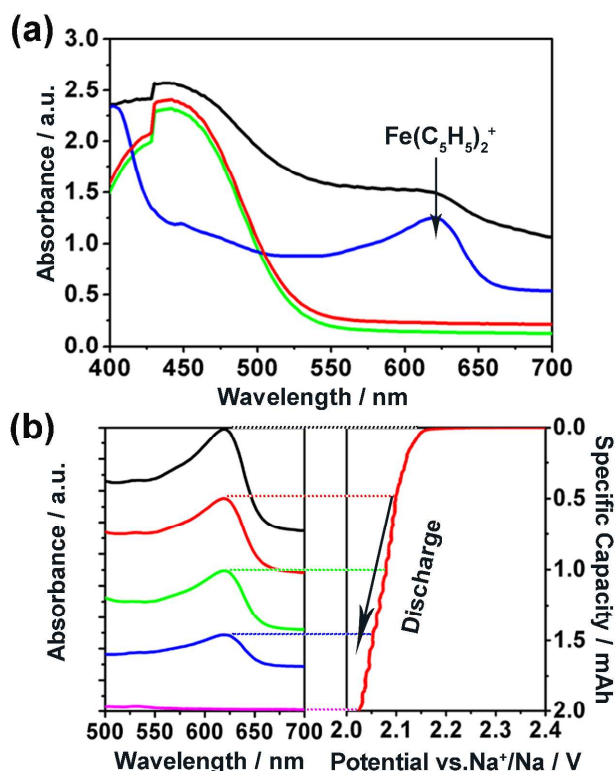


**Fig. 5** (a) UV absorption spectra of the electrolytes with  $\text{Fe}(\text{C}_5\text{H}_5)_2$  after the battery directly charged to 3.5 V (the black line); after the battery discharged to 1.8 V (the red line); after the battery discharged and subsequently recharged to 3.5 V (the green line) at the current density of  $0.05 \text{ mA cm}^{-2}$ ; The datum of the solution with  $\text{Fe}(\text{C}_5\text{H}_5)_2^+$  obtained by the reaction between  $\text{FeCl}_3$  and  $\text{Fe}(\text{C}_5\text{H}_5)_2$  in a faintly acid environment (the blue line) is included for comparison. (b) *Ex situ* UV absorption spectra of the electrolyte at the various discharged states after the battery directly charged to 2.0 mAh in  $0.05 \text{ M Fe}(\text{C}_5\text{H}_5)_2$ -containing electrolyte at the current density of  $0.05 \text{ mA cm}^{-2}$ .

Two different pathways with ferrocene as electrocatalyst and electrochemistry during the charge process might be governed by the morphological feature of the electrode caused by the deposition of  $\text{Na}_2\text{O}_2$  in SABs. In the early stage of the cycles, the active sites on air cathode are not fully covered by  $\text{Na}_2\text{O}_2$  after discharge, as shown in Fig.4b. Therefore, the ferrocene can diffuse to the active sites, subsequently oxidized to  $\text{Fe}(\text{C}_5\text{H}_5)_2^+$ . Such an electrochemistry reaction of  $\text{Fe}(\text{C}_5\text{H}_5)_2$  mainly occurred during charge process in this stage. As the cycle of the cell continues, the morphology of the  $\text{Na}_2\text{O}_2$  varies, as shown in Fig.4b-d. The ferrocene is not able to contact with the air cathode and then cannot be oxidized until the active sites gradually exposed during the decomposition of  $\text{Na}_2\text{O}_2$  under the catalytic influence of ferrocene. At the later stage of the cycles, the electrocatalysis of  $\text{Fe}(\text{C}_5\text{H}_5)_2$  becomes the dominant in driving the decomposition of  $\text{Na}_2\text{O}_2$  during the charge process, resulting in the decreased charge potential. Obviously, dual catalytic behaviors of a soluble ferrocene as electrocatalyst and electrochemistry for SABs should be responsible for the different shapes of charge curves upon cycles. Hence, the morphological control of the discharge product is crucial for an overall performance enhancement in SABs.

## Conclusion

The SAB with a soluble ferrocene as catalyst shows excellent cycle performance of up to 230 cycles with a high capacity of  $1000 \text{ mAh g}^{-1}$ . The ferrocene has dual catalytic activities for the decomposition of discharge products. As a major advantage over the previously reported catalysts, the low cost, and high catalytic, non-toxicity, environmental friendly all make it attractive for SABs.

## Experimental section

### Materials and construction of the cell

1,2-dimethoxyethane (DME)(Acros, 99%) was dried over activated 4A molecular sieves for one week.  $\text{NaClO}_4$ (Alfa Aesar, 98.0%) was dried at  $100^\circ\text{C}$  under a vacuum oven for 24 h.  $\text{Fe}(\text{C}_5\text{H}_5)_2$ (Aladdin,

99%) was used as received. A carbon nanotube (CNT, Chengdu Organic Chemicals Co. Ltd)@Ni electrode was obtained by dispersing CNT powders into ethanol and then casting onto the Ni foam, followed by drying at 75 °C for 24 h.

A conventional two-electrode battery was constructed in the dry air filled glove box with the CNT@Ni as the cathode and one sheet of high-purity sodium foil as the anode. Two kinds of liquid electrolytes were used - one is 1.0 M NaClO<sub>4</sub> in a nonaqueous solution of 1,2-dimethoxyethane (DME) as pristine electrolyte and another is the pristine electrolyte with the addition of 0.05 M Fe(C<sub>5</sub>H<sub>5</sub>)<sub>2</sub>.

### Characterization

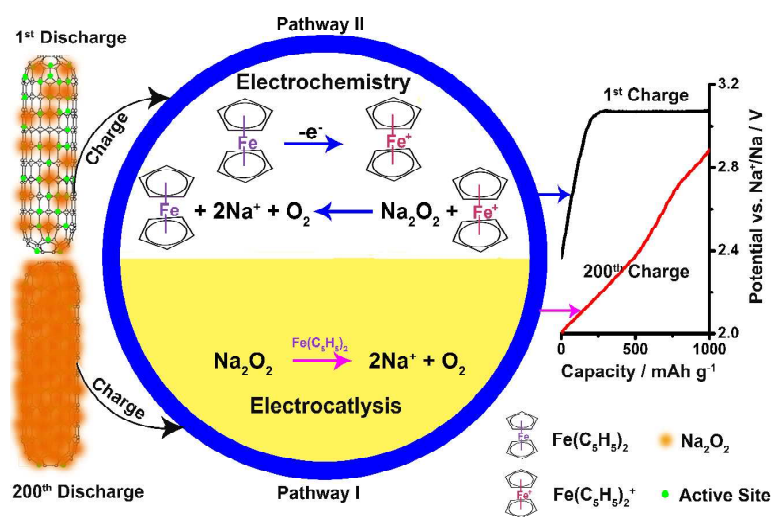
Charge-discharge measurements were performed at room temperature with a Land BT 1-40 battery test system. All discharge/charge capacities were calculated based on the weight of CNT, which was examined by electrobalance (BP211D, Sartorius). Field-emission scanning electron microscopy (FESEM, Cambridge S-360) was employed to study the morphology of the air cathodes. Field-emission transmission electron microscopy (FETEM) and selected-area electron diffraction measurements (SAED) were carried out in a 200 kV side entry JEOL 2010 TEM. *Ex situ* TEM and SAED measurements were collected from air electrodes after initial discharge and charge process. The model cells were disassembled in an Ar-filled glove box and the air electrodes were rinsed by DME for several times to remove the residual sodium salts. To avoid any exposure of air electrodes to oxygen or water, they were rapidly transferred into the chambers for characterization. The Visible absorption spectroscopy was recorded on a 723N visible spectrophotometer.

### Acknowledge

This work was financially supported by the NSAF (Grant No.U1430104), 973 Program (no. 2011CB933300) of China, and Science & Technology Commission of Shanghai Municipality (08DZ2270500 and 11JC 1400500) and National Foundation of China (no. B1120132029).

### References

- 1 R. V. Noorden, *Nature.*, 2014, **507**, 26-28.
- 2 E. Peled, D. Golodnitsky, H. Mazor, M. Goor, S. Avshalomov, *J. Power Sources.*, 2011, **196**, 6835-6840.
- 3 Q. Sun, Y. Yang, Z. W. Fu, *Electrochem Commun.*, 2012, **16**, 22-25.
- 4 W. Liu, Q. Sun, Y. Yang, J. Y. Xie and Z. W. Fu, *Chem. Commun.*, 2013, **49**, 1951-1953.
- 5 Y. L. Li, H. Yadegari, X. F. Li, M. N. Banis, R. Y. Li and X. L. Sun, *Chem. Commun.*, 2013, **49**, 11731-11733.
- 6 Z. Jian, Y. Chen, F. J. Li, T. Zhang, C. Liu and H. S. Zhou, *J. Power Sources.*, 2014, **251**, 466-469.
- 7 W. M. Liu, W. W. Yin, F. Ding, L. Sang and Z. W. Fu, *Electrochem Commun.*, 2014, **45**, 87-90.
- 8 S. Rosenberg, A. Hintennach, *J. Power Sources.*, 2015, **274**, 1043-1048.
- 9 P. Hartmann, C. L. Bender, M. Vracar, A. K. Durr, A. Garsuch, J. Janek and P. Adelhelm, *Nat. Mater.*, 2013, **12**, 228-232.
- 10 P. Hartmann, C. L. Bender, J. Sann, A. K. Durr, M. Jansen, J. Janek and P. Adelhelm, *Phys. Chem. Chem. Phys.*, 2013, **15**, 11661-11672.
- 11 P. Hartmann, D. Grubl, H. Sommer, J. Janek, W. G. Bessler and P. Adelhelm, *J. Phys. Chem. C.*, 2014, **118**, 1461-1471.
- 12 C. L. Bender, P. Hartmann, M. Vracar, P. Adelhelm and J. Janek, *Adv. Energy Mater.*, 2014, **4**, 1301863.
- 13 N. Zhao, C. L. Li and X. X. Guo, *Phys. Chem. Chem. Phys.*, 2014, **16**, 15646-15652.
- 14 W. W. Yin, Zulipiya Shadike, Y. Yang, F. Ding, L. Sang, H. Li and Z.W. Fu, *Chem. Commun.*, 2015, **51**, 2324-2327.
- 15 B. Lee, D. H. Seo, H. D. Lim, I. Park, K. Y. Park, J. Kim and K. Kang, *Chem. Mater.*, 2014, **26**, 1048-1055.
- 16 R. Jiang, X. W. Di, Z. X. He, *Metallurgical Analysis.*, 2006, **26**, 59-61.
- 17 Y. Li, J. Wang, X. Li, D. Geng, M. N. Banis, R. Li and X. Sun, *Electrochem. Commun.*, 2012, **18**, 12-15.
- 18 Y. Li, J. Wang, X. Li, J. Liu, D. Geng, J. Yang, R. Li and X. Sun, *Electrochem. Commun.*, 2011, **13**, 668-672.
- 19 R. R. Mitchell, B. M. Gallant, C. V. Thompson and Y. ShaoHorn, *Energy Environ. Sci.*, 2011, **4**, 2952-2958.
- 20 B. Y. Xia, Y. Yan, X. Wang and X. W. (David) Lou, *Mater. Horiz.*, 2014, **1**, 379-399.
- 21 Y. Liu, M. Wang, L. J. Cao, M. Y. Yang, S. H. S. Cheng, C. W. Cao, K. L. Leung, C. Y. Chung, Z. G. Lu, *J. Power Sources.*, 2015, **286**, 136-144.
- 22 J. Kim, H.D. Lim, H. Gwon and K. Kang, *Phys. Chem. Chem. Phys.*, 2013, **15**, 3623-3629.
- 23 W. G. F. X. X. Guo, D. D. Xiao, and L. Gu, *J. Phys. Chem. C.* 2014, **118**, 7344-7350.



The ferrocene has dual catalytic activities for the decomposition of  $\text{Na}_2\text{O}_2$  in sodium air batteries